GEODESY AND GEODYNAMICS 2015, VOL 6 NO 5, 333–343

Available online at www.sciencedirect.com

ScienceDirect

journal homepage: www.keaipublishing.com/en/journals/geog;
http://www.jgg09.com/jweb_ddcl_en/EN/volumn/home.shtml

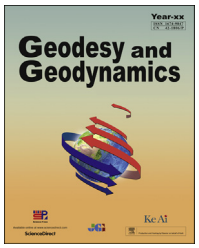

A preliminary study of level 1A data processing of a low–low satellite to satellite tracking mission

Xu Peng[a,b,c], Qiang Li'e[d], Bian Xing[a,e], Dong Peng[a,b], Ju Peng[d], Gao Wei[a,e], Gong Xuefei[a], Luo Ziren[f], Shao Mingxue[b], Tang Wenlin[g], Wan Xiaoyun[h], Lau Yun-Kau[a,b,c,i,*]

[a] Institute of Applied Mathematics, Academy of Mathematics and Systems Science, Chinese Academy of Sciences, Beijing 100190, China
[b] Morningside Center of Mathematics, Chinese Academy of Sciences, Beijing 100190, China
[c] State Key Laboratory of Geodesy and Earth's Dynamics, Institute of Geodesy and Geo-physics, Chinese Academy of Sciences, Wuhan 430077, China
[d] Department of Geophysics, College of the Geology Engineering and Geomatics, Chang'an University, Xi'an 710054, China
[e] University of Chinese Academy of Sciences, Beijing 100049, China
[f] Max-Planck-Institute for Gravitational Physics (Albert Einstein Institute), Hannover, Germany
[g] Aerospace Flight Dynamics Laboratory, Beijing Aerospace Control Center, Beijing 100094, China
[h] Qian Xuesen Laboratory of Launch Vehicle Technology, Beijing 100094, China
[i] State Key Laboratory of Scientific and Engineering Computing, Academy of Mathematics and Systems Science, Chinese Academy of Sciences, Beijing 100190, China

ARTICLE INFO

Article history:
Received 3 June 2015
Accepted 10 August 2015
Available online 9 October 2015

Keywords:
Data processing
Dual-one-way ranging (DOWR)
Gravity recovery and climate experiment (GRACE)
K-band ranging (KBR)
Satellite to satellite tracking (SST)
Noise analysis
Satellite gravity
Ultra stable oscillator (USO)

ABSTRACT

With the Gravity Recovery and Climate Experiment (GRACE) mission as the prime example, an overview is given on the management and processing of Level 1A data of a low–low satellite to satellite tracking mission. To illustrate the underlying principle and algorithm, a detailed study is made on the K-band ranging (KBR) assembly, which includes the measurement principles, modeling of noises, the generation of Level 1A data from that of Level 0 as well as Level 1A to Level 1B data processing.

© 2015, Institute of Seismology, China Earthquake Administration, etc. Production and hosting by Elsevier B.V. on behalf of KeAi Communications Co., Ltd. This is an open access article under the CC BY-NC-ND license (http://creativecommons.org/licenses/by-nc-nd/4.0/).

* *Corresponding author*. Institute of Applied Mathematics, Academy of Mathematics and Systems Science, Chinese Academy of Sciences, Beijing 100190, China.
E-mail address: lau@amss.ac.cn (Lau Y.-K.).
Peer review under responsibility of Institute of Seismology, China Earthquake Administration.

Production and Hosting by Elsevier on behalf of KeAi

http://dx.doi.org/10.1016/j.geog.2015.07.005
1674-9847/© 2015, Institute of Seismology, China Earthquake Administration, etc. Production and hosting by Elsevier B.V. on behalf of KeAi Communications Co., Ltd. This is an open access article under the CC BY-NC-ND license (http://creativecommons.org/licenses/by-nc-nd/4.0/).

1. Introduction

The present work is a continuation of a mission study commissioned by the National Space Science Center of the Chinese Academy of Sciences. The objective of the mission study is to understand various technological as well as scientific aspects of a prospective low–low satellite to satellite tracking (LL-SST) gravity mission in the post Gravity Recovery and Climate Experiment (GRACE) Follow On era, with laser interferometry replacing the microwave ranging in tracking of the range rate variation between two satellites. In China, this prospective mission acquires extra significance of being a stepping stone to another planned mission aiming to detect gravitational wave in space [1].

As part of the feasibility study, a preliminary study is also made on the data structure and management of a LL-SST mission, including both the GRACE type mission using microwave ranging as well as the more advanced type using laser interferometry. The present work is extracted from a report of the study. We will outline a possible basic framework for Level 1A (L1A) data management for future LL-SST mission in China. To illustrate the working principles underlying the 1A data analysis, a more detailed study is made on the K-band ranging (KBR) assembly, with a view that more detailed and comprehensive study including other payloads will be made in future when we have a more concrete plan for the future development of satellite gravity in China. It should be remarked that the materials presented here are not entirely original and appropriate references will be given throughout. Despite of this lack of originality, we feel perhaps it is still useful, particularly for the aerospace industries and the satellite gravity user community in China, to go public our study.

As far as the background of the present work is concerned, very scant knowledge on the details of 1A data processing of the GRACE mission is available in the references [2,3]. Some peripherally related work in this area may also be found in the Chinese references [4–6] together with some discussion on raw data processing [7]. In this work, we will have to start from the basics, build the mathematical models for the payloads ourselves in order to do further analysis and simulations.

The layout of the present work may be given as follows. At first, we give an overview of the data management and processing procedure of a LL-SST mission. The basic framework for the Level 1A data analysis is also reviewed. And then, we present the detailed studies on KBR assembly including the measurement principles, productions of Level 0 (L0) and Level 1A data, noise modelings as well as the processing from Level 1A to Level 1B data. Remarks and future plans are summarized in the last section.

2. Overview of the data management and processing

The main theme of the present work is to give a brief overview of the preprocessing procedures from the L1A to L1B data products of a LL-SST mission, with the GRACE mission as our concrete example. Basically, the preprocessing procedures consist of noise calibration of payloads, identification of anomalous instrumental and environmental events, filtering out errors in data transmission and corrections of biases and systematics. This will enable us to separate out signals from noises and systematics, and then generate the Level 2 (L2) data for scientific purposes. Before doing so, let us first give an overview of the data management of the GRACE mission.

The data products of the GRACE mission are divided into the following three levels [8–11] (see Fig. 1).

a) L0 data (raw data) products: Except for the GPS occulation data, all the raw instrument data is collected by the on board data handling (OBDH) system and transmitted through the S-band channel to the GRACE Raw Data Center (RDC) at Deutsches Zentrum für Luft und Raumfahrt (DLR). In each downlink pass from each satellite, the telemetry data is further divided into two streams, namely, the science instrument data and the spacecraft housekeeping data. Both will and are stored in the rolling archives in the RDC, which are the L0 data product files. The L0 data files contain the unscaled binary instrument data with description headers, which will be documented permanently at the GRACE Science Data System (SDS) centers at Jet Propulsion Laboratory (JPL) and GeoForchungs Zentrum Potsdam (GFZ).
b) L1 data products: The L1 data comprises the KBR assembly data, science instruments (accelerometer (ACC), star camera assembly (SCA) and GPS) data, housekeeping data and intermediate ancillary data, which is further divided into L1A and L1B data products. The L1A data results from the nondestructive processing applied to the L0 data. The L0 binary is converted to engineering units with time tags, editing and quality control flags added. In general, except for the bad data packets, the transition between L0 data to L1A data is reversible. The L1B data results from the destructive irreversible processing applied to both the L1A and L0 data. The L1B data contains the intersatellite biased range, range rate and range acceleration, the non-gravitational accelerations from each satellite, the pointing estimate and orbits.
c) L2 data (science data) products: The L2 data is the science data product generated from L1 B and other ancillary data. Through JPL and GFZ, the monthly Earth gravity field is released in the form of spherical harmonic coefficients, and the mean or static gravity field is also produced by combining several months of data. Some groups also distribute the value-added products (like mass anomalies or water layer) based on the L2 data, which is called the L3 data products [12].

The overview of the GRACE data processing flow is summarized in the flow chart in Fig. 1. The processing from the L0 data product to the L1B data product is called the L1 data processing or preprocessing, which mainly assess the performance of the payloads. The aim of the data preprocessing is to produce, from the calibrated instruments data (L0 and L1A), all the necessary input data (L1B) for the derivations of the monthly time-variation of the Earth's gravity field and mean gravity fields. These involve several processing steps for each instrument (reversible and irreversible), like units conversion, removing the effects from possible anomalous instrumental or environmental events and compressing the propagated instrumental errors which include the time tag corrections,

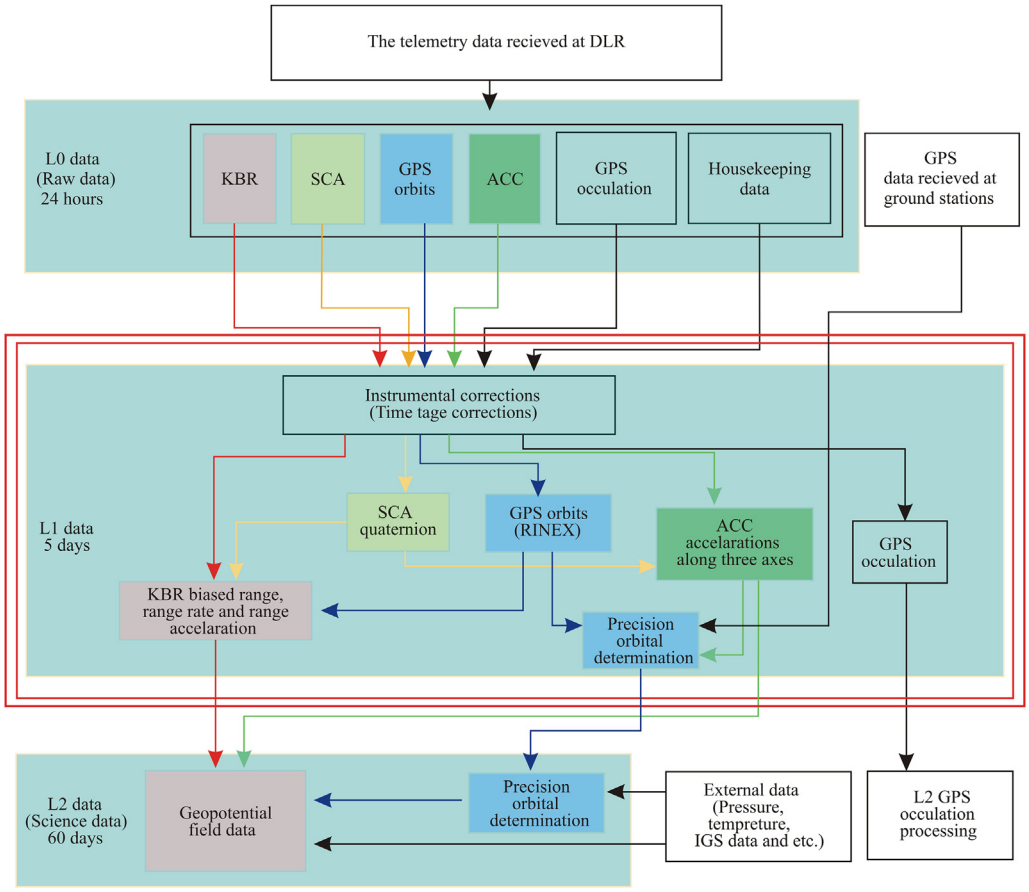

Fig. 1 – The overall flow chart of the GRACE data processing from L0 to L2 products [13].

filtering out possible noises, resamplings at lower rates. We will focus on the data preprocessing procedure enclosed in the double box in the present work.

3. The K-band ranging assembly

3.1. *The measurement principle and noise model*

The KBR assembly is the key science payload of the GRACE satellites, whose Dual-One-Way Ranging (DOWR) measurement generates a key data product. Further, the KBR data needs the most complicated processing. Together with the GPS orbit determination data, the ACC and the SCA data, the DOWR data is used to fit the spherical harmonic coefficients of the geopotential field. In this subsection, we focus on the measurement principle, the noise model of the KBR system and the generation of its L0 and L1A data.

3.1.1. *Measurement principle of the KBR system*

The measurement principle or mathematical model of the KBR system is quite simple. Suppose that there are two oscillators carried by each satellite, S/C *A* and *B*, which are precisely synchronized with each other. Microwave telemetry is employed to compare the phases between this two oscillators. The variations of inter-satellite range can be readout through the phase difference, and such measurement is called the biased range due to the integer wavelength ambiguity [14–16]. To realize such mathematical model, each satellite carries an ultra stable oscillator (USO) as the local frequency standard, which drives the K-band@24.5GHz, the Ka-band@32.7GHz, GPS L-band and also the local receiver clock@19.3MHz signals. Such K/Ka band signals will play the role of the local reference oscillators, which are transmitted and received by a horn on each satellite serving as the antenna. The received K/Ka signal will be compared with the local reference oscillator and be down-converted to the signal with differential phases. This signal is processed and re-sampled by the BlackJack receiver with the differential phase data as the output. See Fig. 2a for illustration [17].

According to the above model, the main noise sources will include the following [2,3,13], see the red parts in Fig. 2b.

a) Noise from the USO instability: The USO as the local frequency standard is one of the key payloads, whose high frequency instability and frequency drift will generate the phase error in the K/Ka signal and time tag error in the output data series.
b) Error from the ionosphere: Due to the disturbance from the inter-satellite media, the speed of the microwave signal differs slightly from the speed of light in vacuum, which will produce an error in the phase data.

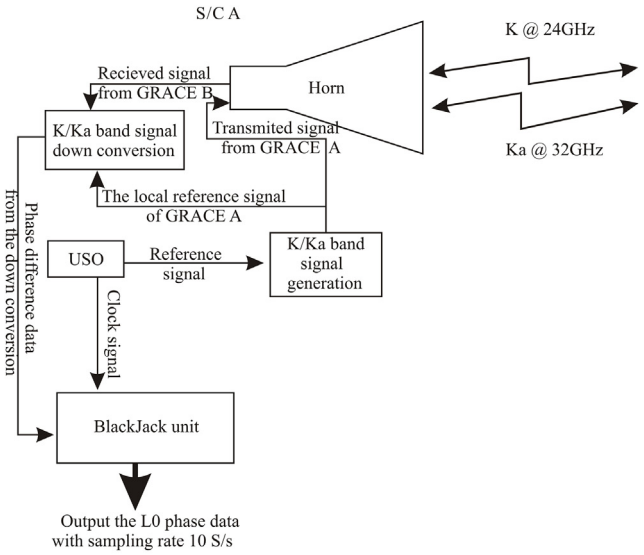

a– The measurement model of the KBR system [2, 17].

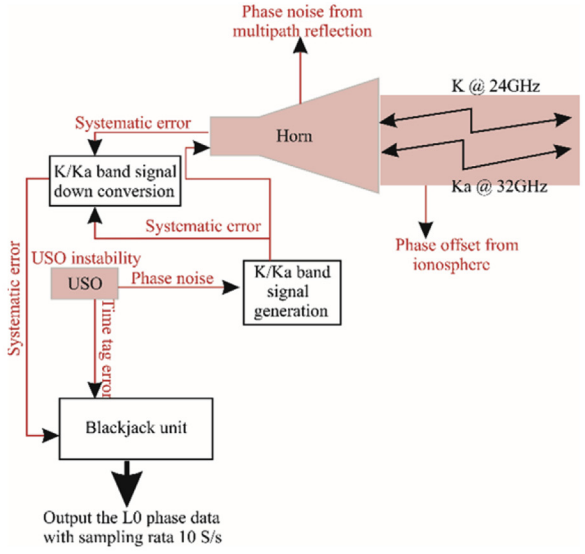

b– The main noise sources in the KBR system.

Fig. 2 – The KBR system.

c) Multipath noise: Due to the errors in the attitude control, the line of sight (LOS), that the straight line between the two satellites' phase center, may not be perfectly parallel to the K/Ka-band bore-sight. Therefore, the microwave signal will be reflected by many times in the horn and gives rise to quite complicated phase noise.
d) Other offset, systematic noises: These include the range error caused by the fly time difference between dual one-way microwaves, systematic noises in the instruments.

3.1.2. *The generation of the L0 data*

The generation of the L0 data of the KBR system is illustrated in Fig. 3. As the first step, the USO generates a signal with frequency f_{USO} = 4.832 MHz. With 5076 and 6768 folds frequency multiplications [2], the K and Ka bands local reference signal are generated and transmitted by the antenna. Hereafter, we take the K-band signal as example, the Ka-band is identical. We write down the transmitted K-band signal as

$$V_A = A_A\cos(\phi_A(t)),\quad V_B = A_B\cos(\phi_B(t)) \tag{1}$$

where $\phi(t)$ denotes the phase and t is the nominal time. The index A, B label the two spacecrafts (S/C), and we use the upper index for the signal received from satellite A/B and the lower index for the signal transmitted by satellite A/B. Due to the instability of the USO, the phase of the K-band signal will not increase linearly with the nominal time. For example, the phase time dependence of the transmitted signal from S/C A may be expanded as [18]

$$\phi_A(t) = \bar{f}_A t + \frac{1}{2}\frac{df_A}{dt}t^2 + \eta_A(t) \tag{2}$$

where the first term is the nominal reference phase $\bar{\phi}_A$ with nominal frequency $\bar{f}_A$, and the rest two terms are the phase error $\delta\phi_A(t)$. Among the error, the quadratic term is the frequency drift mainly caused by the aging of the relevant components, and $\eta_A(t)$ is the random phase noise from the instability of the USO.

Now suppose that, at nominal time t, S/C A receives the K-band signal from S/C B with phase $\phi^B(t) = \phi_B(t - \tau_A^B)$, where τ_A^B is the fly time of the signal from S/C B to A. The received signal reads

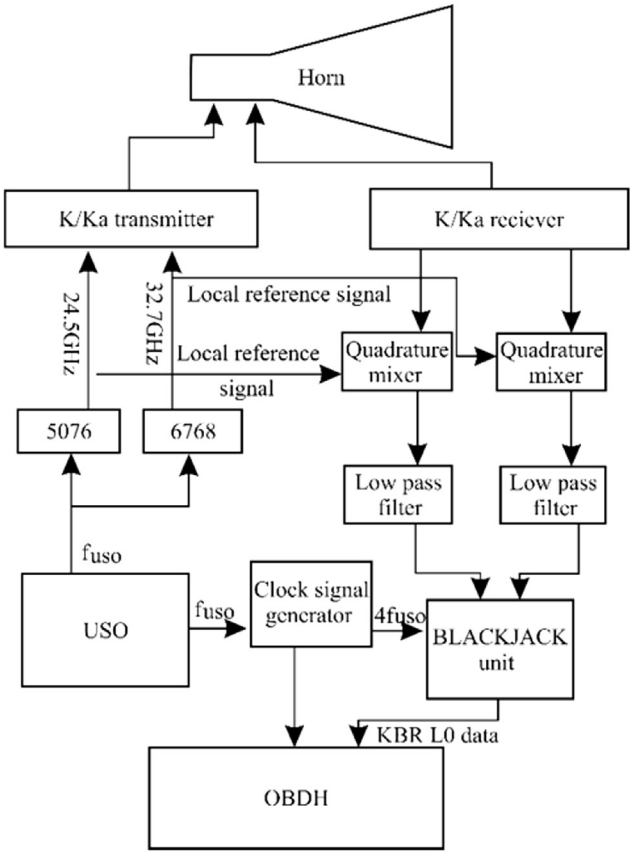

Fig. 3 – The generation of the L0 data of the KBR system [2].

$$V^B = A^B\cos\left(\phi_B(t-\tau_A^B) + I_A^B + d_A^B\right) \tag{3}$$

where I_A^B denotes the error caused by the ionosphere and d_A^B including the systematic noise and the errors from the multipath reflections, and atmosphere.

To obtain the phase difference $\phi_A(t) - \phi^B(t)$ at nominal time t, the local reference signal V_A is used to down-convert the received signal V^B. First, V^B and V_A are input into a quadrature mixer, and then the data $V_A \times V^B$ is obtained which contains two components with frequencies $\bar{f}_A + \bar{f}_B$ and $\left|\bar{f}_A - \bar{f}_B\right|$. The expected signal is the one depends on the phase differences, and to make sure such signal give rise to a periodic function of t, one has to set a non-zero offset between $\bar{f}_A$ and $\bar{f}_B$. For the convenience of signal extraction, one may hope to use a rather bigger offset, but the following analysis shows that the bigger the offset is, the larger the noise from the USO instability in the DOWR data will be. To achieve a balance, the real offset is chosen to be 0.5 MHz in the K-band and 0.67 MHz in the Ka-band. A 9.5 MHz low pass filter (LPF) is then applied to the signal $V_A \times V^B$ to filter out the $\bar{f}_A + \bar{f}_B$ component, then the resulted signal reads

$$V_A^B = A_A^B\cos\left(\phi_A(t) - \phi_B(t-\tau_A^B) + I_A^B + d_A^B + N_A^B\right) \tag{4}$$

where N_A^B denotes the integer-cycle phase ambiguity.

The USO signal with frequency f_{USO} is input into the clock signal generator to give the signal of the local receiver clock with frequency $4f_{USO} = 19.328$ MHz. Through the BlackJack unit, the above signal V_A^B is then sampled and assigned with time tags according to this clock signal. The phase in V_A^B@19.328 MHz is extracted through the digital phaselocked loop (DPLL) [19,20] at the rate of 10 S/s and then delivered to OBDH. This binary values will then be transmitted to the ground stations and be packed into the L0 data of the KBR system.

With some calibrations and units conventions, the L1A phase data of the KBR system for *S/C A* and *S/C B* may be given as

$$\begin{aligned}
\phi_A^B &= \bar{\phi}_A(t+\Delta t_A) + \delta\phi_A(t+\Delta t_A) - \bar{\phi}_B\left(t+\Delta t_A-\tau_A^B\right)\\
&-\delta\phi_B\left(t+\Delta t_A-\tau_A^B\right) + I_A^B + d_A^B + N_A^B + \varepsilon_A^B\\
\phi_B^A &= \bar{\phi}_B(t+\Delta t_B) + \delta\phi_B(t+\Delta t_B) - \bar{\phi}_A\left(t+\Delta t_B-\tau_B^A\right)\\
&-\delta\phi_A\left(t+\Delta t_B-\tau_B^A\right) + I_B^A + d_B^A + N_B^A + \varepsilon_B^A
\end{aligned} \tag{5}$$

where the unit is cycle, $\Delta t_{A/B}$ is the time tag error relative to the nominal time caused by the USO instability and ε denotes the random systematic noise.

3.1.3. *The noise mode*

a) Error from the USO instability: According to the previous analysis and equation (5), the USO instability will cause two kinds of errors in the phase data of the KBR system, that is the phase error and the time tag error. While, in the KBR system, the time and phase measurements are equivalent in nature, since both of these two are in fact counting the oscillation cycles of the USO. The only difference is that the unit of time measurement is second while the unit of phase measurement is cycle. To interchange between these two measurements, we only needs a conversion factor with dimension of cycle/second, which is just the frequency. We then have the simple relation between the time tag error and the phase error [3]

$$\bar{f}_{A/B}\Delta t_{A/B} = \delta\phi_{A/B} \tag{6}$$

Therefore, for the total effects from the USO instability in the KBR phase data, one only needs to know the power spectral density (PSD) of the phase error $S_{\delta\phi}^{K/Ka}(f)$. One can derive the relation between the phase noises of the USO and phase error in the K/Ka-band signal as

$$\begin{aligned}
\delta\phi(t)^{K/Ka}(t) &= 2\pi\bar{f}_{K/Ka}\int_0^t \frac{\delta f_{K/Ka}(t')}{\bar{f}_{K/Ka}}dt'\\
&= 2\pi\bar{f}_{K/Ka}\int_0^t \frac{\delta f_{USO}}{\bar{f}_{USO}}dt'\\
&= \frac{\bar{f}_{K/Ka}}{\bar{f}_{USO}}\delta\phi^{USO}
\end{aligned}$$

Then the relation between the PSDs becomes [18]

$$S_{\delta\phi}^{K/Ka}(f) = \left(\frac{\bar{f}_{K/Ka}}{\bar{f}_{USO}}\right)^2 S_{\delta\phi}^{USO}(f)$$

The f^{-n} fit of the PSD of the on-board USO reads [2,18]

$$\begin{aligned}
S_{\delta\phi}^{USO}(f) = \frac{1}{4\pi^2}\Bigg(&3.16\times10^{-16} + \frac{8.38\times10^{-13}}{f^2} + \frac{5.74\times10^{-14}}{f^3}\\
&+\frac{6.39\times10^{-17}}{f^4}\Bigg)
\end{aligned} \tag{7}$$

Please see Fig. 4 for the illustrations of $S_{\delta\phi}^{USO}(f)$ and $S_{\delta\phi}^{K/Ka}(f)$.

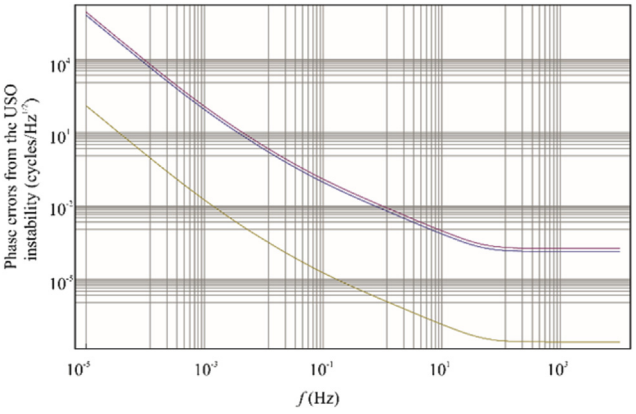

Fig. 4 – The blue curve stands for the root PSD of the phase error in the K band, the red one for the Ka band, and the brown curve for the USO.

b) Error from the ionosphere: The K/Ka-band signal will be slightly delayed by the free electric charges along the path. For the case of rarefied charge density, the corresponding phase shift or the phase error will depend linearly on the total electron content (TEC) along the path [2,21]

$$I_A^B = \frac{TEC_A^B}{f_B} \tag{8}$$

where TEC depends on the actual state of the ionosphere and varies from epoch to epoch.

c) Multipath errors: Because of the arbitrary geometric configurations between the two satellites, there is no general model of multipath errors. But, if the attitude control system can fulfill the requirements, that the relative orientations between the two satellites are within certain boundaries, the biased range error from multipath reflections is below 1 μm according to numerical simulations [3] and may be neglected.

d) Systematic noises: The systematic noise mainly contains the background noise and the thermal noise, which is white and has the form

$$\varepsilon = \frac{1}{2\pi SNR_V} \tag{9}$$

The voltage signal-to-noise ratio (SNR) for the BlackJack receiver in quadrature down-conversion and samplings is about 2800 in 1s. Therefore the 1s systematic noise ε is about 57μcycle.

3.2. *The preprocessing from L1A data to L1B data*

The main task of the preprocessing of the KBR phase data is to correct the biases, offsets, compress the noises, and to derive the inter-satellite biased range, range rate and range acceleration from the phase data [9,10]. The overview of the processing flow from L1A data to L1B data of the KBR system is summarized in Fig. 5.

3.2.1. *Time tag error*

The time tag error corrections may be divided into two steps. The first step is rather straightforward. We need to identify the hardware and software problems in the data, like missed interrupts in instruments processing unit (IPU) and constant offsets produced by onboard software, and record them in the sequence of events (SOE). Quality flags are assigned to the data series and the errors caused by such events are corrected [13].

The second step is to correct the time tag errors originated from the noise in the local clock signal generated by the USO, with the help of GPS measurements. Since the data analysis of GPS measurements have been widely studied [21,22], here we only summarize the principles for the correction method. Analogous to the K/Ka-band receiver model equations (4) and (5), the down-converted differential phase of the L-band signal at receiver a from GPS satellite p reads [21,22]

$$\phi_a^p(t+\Delta t_a) = \phi_a(t+\Delta t_a) - \phi^p(t+\Delta t_a) + N_a^p + d_a^p + \varepsilon_a^p$$

where time t is the local time of the receiver. For receivers a, b, and GPS satellites p, q, we define the combined data

$$\phi_{ab}^p(t) = \phi_a^p(t+\Delta t_a) - \phi_b^p(t+\Delta t_b)$$

$$\phi_{ab}^{pq}(t) = \phi_{ab}^p(t) - \phi_{ab}^q(t)$$

and then

$$\begin{aligned}\phi_{ab}^{pq}(t) =& \frac{\bar{f}}{c}\left[\rho_a^p(t) - \rho_b^p(t) - \rho_a^q(t) + \rho_b^q(t)\right] \\ &+ \frac{\bar{f}}{c}\left[\left(\dot{\rho}_a^p(t) - \dot{\rho}_a^q(t)\right)\Delta t_a - \left(\dot{\rho}_b^p(t) - \dot{\rho}_b^q(t)\right)\Delta t_b\right] \\ &+ \frac{\delta f_p}{c}\left[\rho_a^p(t) - \rho_b^p(t)\right] - \frac{\delta f_q}{c}\left[\rho_a^q(t) - \rho_b^q(t)\right] + \frac{\delta f_p}{c}\left[\left(\dot{\rho}_a^p(t) - \dot{\rho}_b^p(t)\right)\Delta t_a\right] \\ &- \frac{\delta f_p}{c}\left[\left(\dot{\rho}_a^q(t) - \dot{\rho}_b^q(t)\right)\Delta t_b\right] - \left(\delta f_p - \delta f_q\right)\left(\Delta t_a - \Delta t_b\right) \\ &+ N_{ab}^{pq} + d_{ab}^{pq} + \varepsilon_{ab}^{pq}\end{aligned}$$

here, ρ_a^p is the instantaneous range between the GPS satellite p and receiver a, $\bar{f}$ is the nominal frequency of the L-band signal. The on-board clocks of GPS satellites are quite stable and their frequency instabilities $\delta f/\bar{f} \le 10^{-12}$ [21,22], therefore the error terms proportional to δf in the above equation may be neglected. Except the noise in the last line, the combined data $\phi_{ab}^{pq}(t)$ will then only depend on the inter-satellite range, range rates and the receiver clock errors Δt. GRACE satellites can, at the same time, receive signals from at most 11 GPS satellites. By means of multi-satellites orbit determination method [23], we can fit the orbits of the GRACE satellites and at the same time also fit out the GRACE local clock error Δt relative to the GPS time.

3.2.2. *The DOWR data*

According to the measurement principle in subsec 3.1.1, the phase errors from the two USOs will be transferred into both the differential phase data ϕ_B^A and ϕ_A^B of the two satellites, see equation (5). Therefore, after the corrections of time tag error, combining the KBR differential phase data of the two satellites with the same nominal time will compress effectively the phase error with correlation time longer than the signal fly time τ. τ is about 1 ms, therefore phase errors below 1 kHz will be compressed.

Again, we take the K-band data for example. First, we combine the two differential phases to the dual one-way phase

$$\begin{aligned}\Phi_{AB}(t) &= \phi_B^A(t) + \phi_A^B(t) \\ &= \left(\bar{f}_A\tau_B^A + \bar{f}_B\tau_A^B\right) + \left(\delta f_A\tau_B^A + \delta f_B\tau_A^B\right) + \left(\bar{f}_A - \bar{f}_B\right)\left(\Delta t_A - \Delta t_B\right) \\ &\quad + \left(\delta f_A - \delta f_B\right)\left(\Delta t_A - \Delta t_B\right) + \left(I_B^A + I_A^B\right) + \left(d_B^A + d_A^B\right) \\ &\quad + \left(N_B^A + N_A^B\right) + \left(\varepsilon_B^A + \varepsilon_A^B\right)\end{aligned} \tag{10}$$

where the following linear expansions have been used in the derivation of the above equation.

$$\bar{\phi}(t+\Delta t-\tau) \simeq \bar{\phi}(t) + \bar{f}\Delta t - \bar{f}\tau$$

$$\delta\phi(t+\Delta t-\tau) \simeq \delta\phi(t) + \delta f\Delta t - \delta f\tau$$

The first term in equation (10) is the phase to be measured, the second term comes from the phase error and the third term

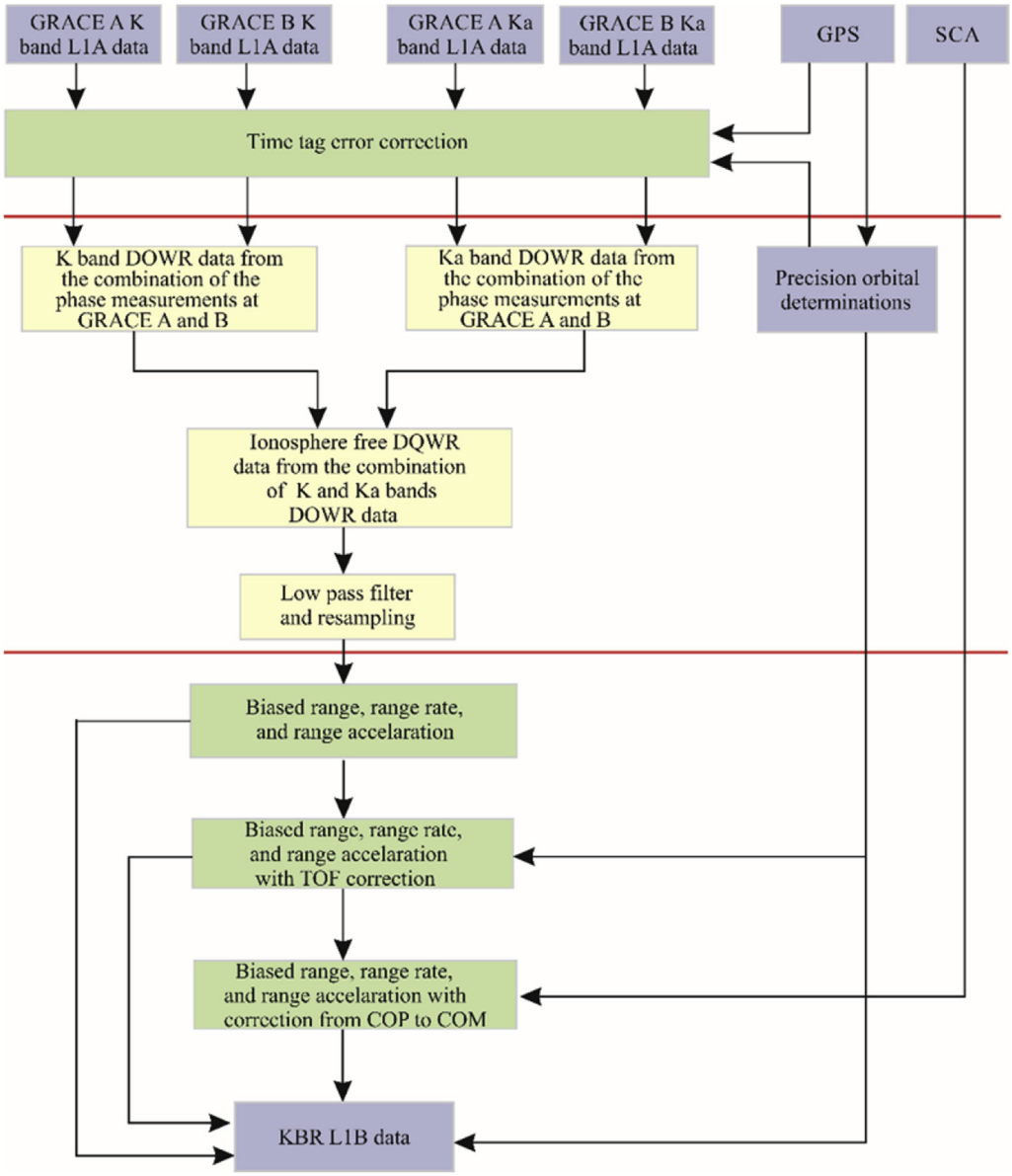

Fig. 5 – Flow chart of processing from L1A data to L1B data for the KBR system.

from the time tag error. Since the time tag error have already been corrected by the GPS time in the last step, its residual error is far smaller and will be neglected. The fourth term is the coupled effect of the phase error and time tag error which is also ignored. At last, the difference $\left|\tau_B^A - \tau_A^B\right|$ is about 0.005 μs, which is much smaller than the time of flight (TOF) which is about 1 ms. Therefore, we can approximately set the TOF $\tau_B^A = \tau_A^B = \tau$, and denote the phase error from such approximation as $\Delta\Phi_{AB}^{TOF}$. Then equation (10) may be rewritten as

$$\Phi_{AB}(t) = \left(\bar{f}_A + \bar{f}_B\right)\tau - \Delta\Phi_{AB}^{TOF} + \left(\delta f_A + \delta f_B\right)\tau + \left(I_B^A + I_A^B\right) + \left(d_B^A + d_A^B\right) + \left(N_B^A + N_A^B\right) + \left(\varepsilon_B^A + \varepsilon_A^B\right)$$

The K-band DOWR data then reads

$$\begin{aligned} R(t) &= \frac{c}{\bar{f}_A + \bar{f}_B}\Phi_{AB} \\ &= \rho(t) - \Delta\rho^{TOF}(t) + c\frac{\delta f_A + \delta f_B}{\bar{f}_A + \bar{f}_B}\tau \\ &\quad + \frac{c}{\bar{f}_A + \bar{f}_B}\left[\left(I_B^A + I_A^B\right) + \left(d_B^A + d_A^B\right) + \left(N_B^A + N_A^B\right) + \left(\epsilon_B^A + \epsilon_A^B\right)\right] \end{aligned} \tag{11}$$

The Ka-band DOWR data is the same. The correction $\Delta\rho^{TOF}$ from the TOF approximation will be derived in the 5th step.

To verify the efficiency of the phase error compression in the DOWR data, we now work out the transfer function of the USO instability noise. To be conservative, we do not ignore the time tag error and the coupled error, that the third and fourth terms in equation (10), in the following analysis. According to equation (6), all the errors $\delta\Phi_{AB}^{USO}(t)$ from the USO instability in

the dual one-way phase may be rewritten only in terms of the phase error $\delta\phi$

$$\delta\Phi_{AB}^{USO}(t)=\left[(\delta\phi_A(t)-\delta\phi_A(t-\tau))-\left(\bar{f}_A-\bar{f}_B\right)\left(\frac{\delta\phi_A}{\bar{f}_A}\right)\right]+\left[(\delta\phi_B(t)-\delta\phi_B(t-\tau))-\left(\bar{f}_A-\bar{f}_B\right)\left(\frac{\delta\phi_B}{\bar{f}_B}\right)\right] \tag{12}$$

The expressions in the two square brackets have the same form, and we denote them as $\delta\Phi_A^{USO}$ and $\delta\Phi_B^{USO}$. Take S/C A as example, the transfer function from the phase error to the dual one-way phase error reads

$$\sqrt{G_A(f)}=\frac{\mathscr{F}\left[\delta\Phi_A^{USO}(t)\right]}{\mathscr{F}\left[\delta\phi_A(t)\right]}=\left(\frac{\bar{f}_B}{\bar{f}_A}-e^{-2\pi i f\tau}\right) \tag{13}$$

where $\mathscr{F}[\cdot]$ denotes the Fourier transformation. For TOF τ is about 1 ms, we give the plots of this dual one-way filter in Fig. 6. As we may see, the low frequency noise from the USO instability will be effectively compressed, and its efficiency increases as the frequency offset $\left|\bar{f}_B-\bar{f}_A\right|$ decrease. But, as mentioned in subsec 3.1.2, a smaller offset will make the extraction of the differential phase more difficult, and to make a balance between these two, the real offset is chosen as 0.5 MHz in the K-band and 0.67 MHz in the Ka-band. In Fig. 7 we show the root PSD of the total phase error $\delta\Phi_{AB}^{USO}(t)$ with frequency offset of 0.5 MHz, and compared with Fig. 4 one can see that the low frequency phase error in the dual one-way phase data does reduce to the required level.

3.2.3. *Elimination of error caused by ionosphere*

From equation (8) and equation (11), the range error caused by the ionosphere reads

$$\Delta\rho^{iono}=\frac{c}{\bar{f}_A+\bar{f}_B}\left(I_B^A+I_A^B\right)=\frac{c}{\bar{f}_A+\bar{f}_B}\left(\frac{TEC_B^A}{\bar{f}_A}+\frac{TEC_A^B}{\bar{f}_B}\right)=\frac{cTEC}{\hat{f}^2} \tag{14}$$

where $\hat{f}=\sqrt{\bar{f}_A\bar{f}_B}$ and in the derivation of the last equals we make use of the approximation that $TEC_B^A=TEC_A^B=TEC$. Combining the dual one-way phase data of both K and Ka-band, we then eliminate the dependence of *TEC* in the range

$$\begin{aligned}\mathscr{R}(t)&=\frac{\hat{f}_K^2R_K(t)-\hat{f}_{Ka}^2R_{Ka}(t)}{\hat{f}_K^2-\hat{f}_{Ka}^2}\\&=\rho(t)+\Delta\rho^{USO}+\frac{\hat{f}_K^2\Delta\rho_K^{system}(t)-\hat{f}_{Ka}^2\Delta\rho_{Ka}^{system}(t)}{\hat{f}_K^2-\hat{f}_{Ka}^2}\\&\quad-\frac{\hat{f}_K^2\Delta\rho_K^{TOF}(t)-\hat{f}_{Ka}^2\Delta\rho_{Ka}^{TOF}(t)}{\hat{f}_K^2-\hat{f}_{Ka}^2}+\frac{\hat{f}_K^2\Delta\rho_K^{other}(t)-\hat{f}_{Ka}^2\Delta\rho_{Ka}^{other}(t)}{\hat{f}_K^2-\hat{f}_{Ka}^2}\end{aligned} \tag{15}$$

where

$$\Delta\rho_{K/Ka}^{system}(t)=\left(\frac{c}{\bar{f}_A+\bar{f}_B}\left(\varepsilon_B^A+\varepsilon_A^B\right)\right)_{K/Ka}$$

$$\Delta\rho_{K/Ka}^{other}=\left[\frac{c}{\bar{f}_A+\bar{f}_B}\left(\left(d_B^A+d_A^B\right)+\left(N_B^A+N_A^B\right)\right)\right]_{K/Ka}$$

Now, let us carefully look at the error terms in equation (15). From the previous analysis, the range errors caused by USO instability $\Delta\rho_K^{USO}$ and $\Delta\rho_{Ka}^{USO}$ for the K and Ka-bands are not independent random variables, but are different multiples of the same random variable $\delta\phi^{USO}$. Therefore, ignoring the frequency offset between the two satellites, we have the second error term $\rho^{USO}=\Delta\rho_K^{USO}=\Delta\rho_{Ka}^{USO}$. For the third term, we have ε equal 57μcycle from equation (9), thus $\Delta\rho_K^{system}$ and $\Delta\rho_{Ka}^{system}$ are about 0.5 μm. The fourth term comes from the TOF difference, and may be precisely corrected in the 5th step. The fifth term, based on previous analysis, is much smaller than the systematic range errors and may be neglected. Finally, at this stage, the PSD of the total noise in the ionosphere free DOWR data reads

$$S_{\Delta\rho}^{total}(f)=\frac{1}{8\pi^2}\left(\frac{c}{\bar{f}_{USO}}\right)^2G(f)S_{\delta\phi}^{USO}+\frac{c^2}{2}\frac{\hat{f}_K^2+\hat{f}_{Ka}^2}{\left(\hat{f}_K^2-\hat{f}_{Ka}^2\right)^2}S^{\varepsilon}(f) \tag{16}$$

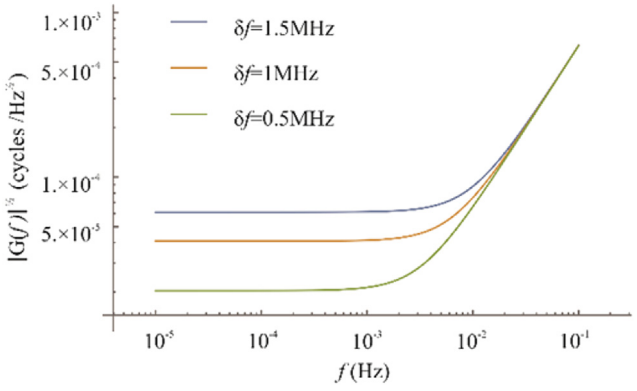

Fig. 6 – The transfer function that map the phase error in the differential phase data to the dual one-way phase data.

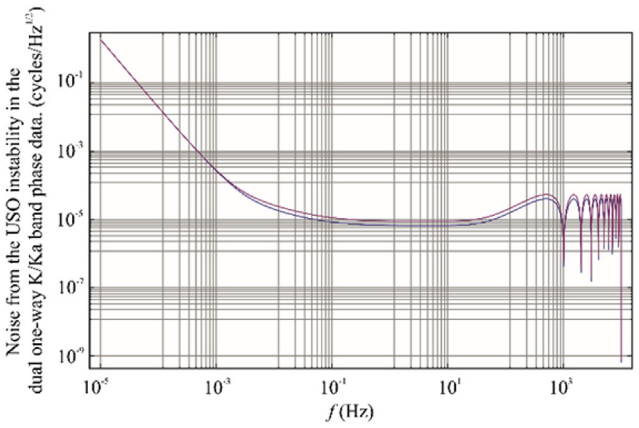

Fig. 7 – The blue/red curve stands for the root power spectral density (PSD) of the noise from the USO instability in the dual one-way K/Ka band phase data.

In Fig. 8, we give the root PSD of the total noise, and in Fig. 9 we compare the noise power before and after processing.

3.2.4. *The low pass filter*

The sampling rate of the L1B data will be reduced from 10 Hz (L1A) to 0.2 Hz. During the re-sampling, the high frequency noise will enter into the Earth gravity field signal band due to the aliasing effect. Therefore, a low pass filter (LPF) has to be employed to further filter out the high frequency noises to prevent this ambiguity. There are different choices of such LPF, but some elementary requirements must be satisfied, that the error produced by the LPF in the gravity field signal band must be smaller than 1 μm, and for the sake of the derivations of range rate and range acceleration the LPF must has explicit analytic expression.

3.2.5. *TOF correction [3]*

The two satellites of GRACE mission are almost following the same polar orbit. Let's denote the leading satellite as S/C A. Then the TOF τ_B^A from S/C A to B will be smaller than τ_A^B from S/C B to A. Neglecting the already corrected errors, equation (11) now reads

$$R(t) = \frac{\bar{f}_A \rho_B^A(t) + \bar{f}_B \rho_A^B(t)}{\bar{f}_A + \bar{f}_B} = \rho(t) - \Delta\rho^{TOF}(t) \tag{17}$$

where $\rho_B^A = c\tau_B^A$, $\rho_A^B = c\tau_A^B$ are the measured ranges, and $\rho(t)$ is the instantaneous range will be used in the gravity field recovering task. Please see Fig. 10 for their geometric relations, where $\mathbf{r}_{A/B}(t)$ is the position vector of S/C A/B at nominal time t, $\boldsymbol{e} = (\boldsymbol{r}_A - \boldsymbol{r}_B)/|\boldsymbol{r}_A - \boldsymbol{r}_B|$ is the unite vector along the LOS at time t from S/C B to A, $\boldsymbol{\Delta}_A = \dot{\boldsymbol{r}}_A \tau_B^A$ is the displacement vector of S/C A during the TOF τ_B^A and $\boldsymbol{\Delta}_B = \dot{\boldsymbol{r}}_B \tau_A^B$ is the corresponding displacement of S/C B. According to Fig. 10, we have

$$\rho_B^A = |\boldsymbol{\rho} - \boldsymbol{\Delta}_A|, \quad \rho_A^B = |\boldsymbol{\rho} + \boldsymbol{\Delta}_B| \tag{18}$$

As $\frac{\Delta_{A/B}}{\rho}$ is about 3×10^{-5}, the above relations can be expanded as

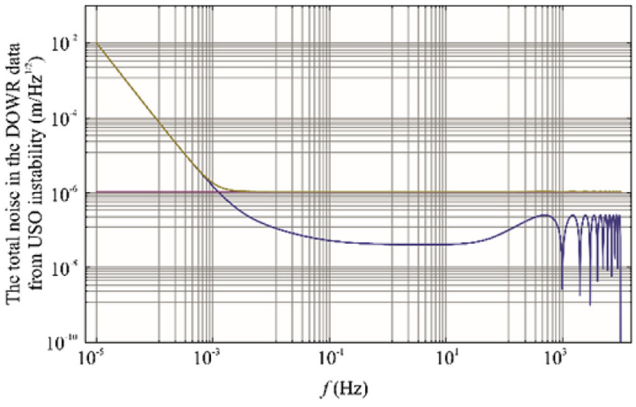

Fig. 8 – The blue curve stands for the root PSD of the noise from the USO instability in the DOWR data. The red line stands for the root PSD of the systematic noise. The brown curve stands for the root PSD of total noise.

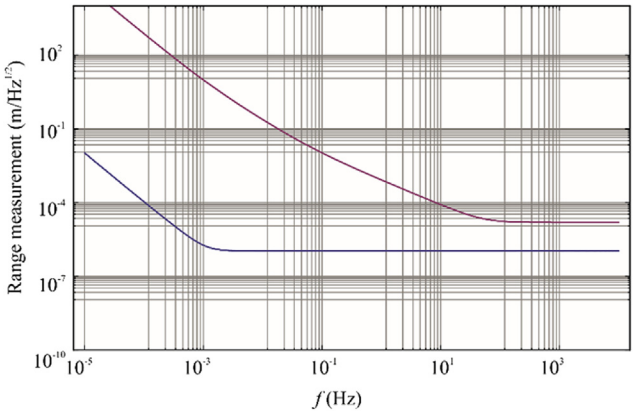

Fig. 9 – The blue/red curve stands for the root PSD of the total noise after/before the processing.

$$\rho_B^A = \rho - \tau_B^A \boldsymbol{e}\cdot\dot{\boldsymbol{r}}_A, \quad \rho_A^B = \rho + \tau_A^B \boldsymbol{e}\cdot\dot{\boldsymbol{r}}_B$$

Substituting ρ_B^A and ρ_A^B into equation (17), the correction reads

$$\Delta\rho^{TOF} = \left(\frac{\bar{f}_A}{\bar{f}_A + \bar{f}_B}\tau_B^A \boldsymbol{e}\cdot\dot{\boldsymbol{r}}_A - \frac{\bar{f}_B}{\bar{f}_A + \bar{f}_B}\tau_A^B \boldsymbol{e}\cdot\dot{\boldsymbol{r}}_B\right)$$

According to the accuracy of the GPS orbit determinations, we have the estimations of the magnitudes and the errors of the following quantities

$$\begin{array}{ll} |\boldsymbol{e}| = 1, & |\delta\boldsymbol{e}| \le 5 \times 10^{-8}\ , \\ |\dot{\boldsymbol{r}}| \le 7700\text{m/s}, & |\delta\dot{\boldsymbol{r}}| \le 10^{-4}\text{m/s}, \\ \tau \le\ 0.001\text{s}\ , & |\delta\tau| \le 10^{-11}\text{s} \end{array}$$

Therefore the residual error in $\Delta\rho^{TOF}$ is rather small.

$$\delta\Delta\rho^{TOF} \simeq |\delta\boldsymbol{e}||\dot{\boldsymbol{r}}||\tau| + |\boldsymbol{e}||\delta\dot{\boldsymbol{r}}||\tau| + |\boldsymbol{e}||\dot{\boldsymbol{r}}||\delta\tau| \le 8 \times 10^{-7}\text{m} \le 1\mu\text{m}$$

3.2.6. *Reduction to the range with respect to COM [3]*

Up to this step, all the biased range data obtained are defined with respect to the centers of phase (COP) of the two satellites. For gravity field recovery, the ranging data relative to the centers of mass (COM) of the two satellites must be obtained. The geometrical relations between COPs and COMs may be found in Fig. 11, from which the range relative to COMs reads

$$R_{COM} = dr_A + r + dr_B$$

where $dr_{A/B}$ is the projection along the LOS of the vector $\mathbf{PC}_{A/B}$ pointing from $COM_{A/B}$ to $COP_{A/B}$, and r is the projection along

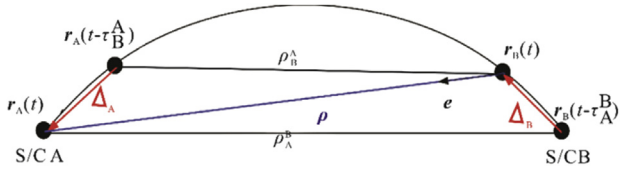

Fig. 10 – Geometric relations between the instantaneous range and the measured ranges [3].

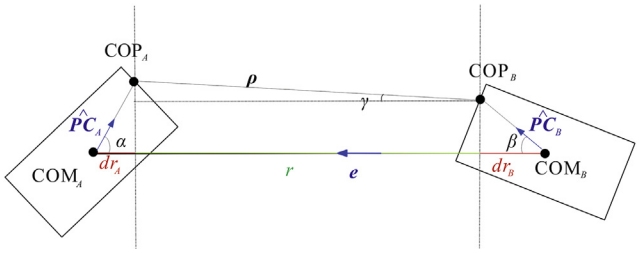

Fig. 11 – Geometric relations between COPs and COMs [3].

the LOS of the instantaneous range $\rho(t)$ with respect to COPs. The three angles in Fig. 11 satisfy

$$\cos\alpha = \boldsymbol{e}\cdot\widehat{\mathbf{PC}}_{\mathrm{A}}$$

$$\cos\beta = \boldsymbol{e}\cdot\widehat{\mathbf{PC}}_{\mathrm{B}}$$

$$\cos\gamma = \boldsymbol{e}\cdot\widehat{\mathbf{PC}}_{\mathrm{AB}}$$

$$\widehat{\mathbf{PC}}_{\mathrm{AB}} = \frac{\boldsymbol{r}_{\mathrm{A}} + \mathbf{PC}_{\mathrm{A}} - \boldsymbol{r}_{\mathrm{B}} - \mathbf{PC}_{\mathrm{B}}}{|\boldsymbol{r}_{\mathrm{A}} + \mathbf{PC}_{\mathrm{A}} - \boldsymbol{r}_{\mathrm{B}} - \mathbf{PC}_{\mathrm{B}}|}$$

where the values of the unit vectors $\widehat{\mathbf{PC}}_{\mathrm{A}}$, $\widehat{\mathbf{PC}}_{\mathrm{B}}$, and $\widehat{\mathbf{PC}}_{\mathrm{AB}}$ are readout by the on-board star trackers with error $\delta\widehat{\mathbf{PC}} \le 5\times10^{-8}$m. Since $r = \rho\cos\gamma$ and $\cos\gamma \le \frac{|\mathbf{PC}|}{\rho}$ is about 10^{-6}, the error in r can be neglected and the residual error in R_{COM} comes from the projections $dr_{\mathrm{A/B}}$

$$\begin{aligned}\delta R_{\mathrm{COM}} &= \delta dr_{\mathrm{A}} + \delta dr_{\mathrm{B}}\\ &\simeq 2\left(|\delta\mathbf{PC}_{\mathrm{A}}|\cos\alpha + |\mathbf{PC}_{\mathrm{A}}|\left(\left|\delta\boldsymbol{e}\cdot\widehat{\mathbf{PC}}_{\mathrm{A}}\right| + \left|\boldsymbol{e}\cdot\delta\widehat{\mathbf{PC}}_{\mathrm{A}}\right|\right)\right)\\ &\simeq 0.5\mu\mathrm{m}\end{aligned}$$

3.2.7. *The L1B data output*

From step 2 to step 6 in the processing, three groups of data will be obtained, that is the ionosphere free DOWR data, the TOF corrected ionosphere free DOWR data and the TOF corrected ionosphere free DOWR data with respect to the COMs. All these three groups of data, together with their quality flags, SNR information will be packed into the L1B data products of the KBR system.

4. Conclusion and future plans

The present work constitutes a very primitive study of L1A data analysis for future satellite gravity mission in China. Dependent on the progress of the satellite gravity program in China, more in depth and widening in scope will be made on the study based on the framework outlined here. At the same time, we would also like to look at alternative processing strategies so that more quality scientific data may be provided to the user community. All these remain work for the future.

Acknowledgments

The present work is a continuation to the project entitled "Advanced Gravity Measurement in Space" supported by the National Space Science Center, Chinese Academy of Sciences Profs. Wenrui Hu and Houze Xu's effort to promote satellite gravity research in China motivated the feasibility study in the first place. Support from National Natural Science Foundation of China (11305255, 11171329 and 41404019) as well as funding from State Key Laboratory of Geodesy and Earth's Dynamics, Institute of Geodesy and Geophysics, Chinese Academy of Sciences (SKLGED2013-3-8-E) are acknowledged.

REFERENCES

[1] Gong X, Lau YK, Xu S, Amaro-Seoane P, Bai S, Cao ZJ, et al. Descope of the ALIA mission. J Phys Conf Ser 2015;610:12011. arXiv:1410.7296 [gr-qc].
[2] Thomas JB. An analysis of gravity-field estimation based on intersatellite dual-1-way biased ranging. Tech. Rep. JPL Publication; 1999. 98–15.
[3] Kim J. Simulation study of a low–low satellite-to-satellite tracking mission. Doctor of philosophy, Graduate School, University of Texas at Austin. 2000.
[4] Xuhua Zhou, Houtse Hsu, Bin Wu, Bibo Peng, Yang Lu. Earth's gravity field derived from GRACE satellite tracking data. Chin J Geophys 2006;49:651 [in Chinese].
[5] Yun Xiao, Renzhe Xia, Xingtao Wang. Recovering the earth gravity field from inter-satellite range-rate of GRACE. Acta Geod Cartogr Sinica 2007;36:19 [in Chinese].
[6] Wei Zheng, Houtse Hsu, Min Zhong, Meijuan Yun, Xuhua Zhou, Bibo Peng. Effective processing of measured data from GRACE key payloads and accurate determination of Earth's gravitational field. Chin J Geophys 2009;52:1966 [in Chinese].
[7] Kang K, Li H, Zou Z, Wu Y. Simulation of measurements and preprocessing technology for high accurate inter satellite microwave ranging system. J Geodesy Geodyn 2011;31:71.
[8] Michael TG, Watkins M, Bettadpur SV. GRACE science data system development plan. Jet Propulsion Laboratory, GeoForchungs Zentrum Potsdam and Center for Space Research Tech. Rep. GRACE 2000; 327–710.
[9] Bettadpur S. GRACE-product Specification Document. Tech. Rep. GRACE 2007; 327–720 (CSRGR-03-02).
[10] Case K, Kruizinga G, Wu SC. GRACE level 1B data product user Handbook. Jet Propulsion Laboratory, California Institute of Technology, Tech. Rep, 2010; JPL D-22027.
[11] Bettadpur S. GRACE-Level-2 gravity field product user Handbook. Center for Space Research, Tech. Rep 2007; GRACE 327–734 (CSR-GR-03-01).
[12] Http://icgem.gfz-potsdam.de/ICGEM/ICGEM.html, http://geoid.colorado.edu/grace/ and http://grace.jpl.nasa.gov.
[13] Frommknecht B. Integrated sensor analysis of the GRACE Mission—an analysis of the GRACE sensor system components and their interaction. Sudwestdeutscher Verlag fur Hochschulschriften; 2009.
[14] Wolff M. Direct measurements of the earth's gravitational potential using a satellite pair. J Geophys Res 1969;74:5295.
[15] Pisacane VL, Ray JC, MacArthur JL, Bergeson-Willis SE. Description of the dedicated gravitational satellite mission (GRAV SAT). IEEE Trans Geoscience Remote Sens 1982; 20:315.

[16] MacArthur JL, Posner AS. Satellite-to-satellite range-rate measurement. IEEE Trans Geoscience Remote Sens 1985;23:517.
[17] GRACE Meeting Presentation GRACE preliminary design review. 1998.
[18] Meditch J. Clock error models for simulation and estimation. Aerospace Report TOR-0076(6474–D1)-2. El Segundo, California: The Aerospace Corporation; 1975.
[19] Thomas JB. An analysis of digital phase-Locked loops, 89. JPL Publication; 1989. p. 2.
[20] Stephens SA, Thomas JB. Controlled-root formulation for digital phase-locked loops. IEEE Trans Aerosp Electron Syst 1995;31:78.
[21] Leick A. GPS satellite surveying. 2nd ed. John Wiley & Sons; 1995.
[22] Hofmann-Wellenhof LHB, Collins J. GPS theory and practice. 3rd ed. Verlag: Springer; 1994.
[23] Tapley BD. In: Tapley BD, Szebehely V, editors. Statistical orbit determination theory39. Recent Advances in Dynamical Astronomy, Astrophysics and Space Science Library; 1973. p. 396.

Xu Peng. From 1999 to 2003, he studied at the School of Physical Science and Technology in Lanzhou University and obtained his bachelor's degree in the theoretical physics majors. From 2003, he studied at Center of Relativity and Gravitation of Beijing Normal University, and received his doctor's degree in 2010. His Ph.D dissertation is on the experimental tests of relativistic gravitational theories in space and loop quantum gravity. He then worked as a postdoc at the Academy of Mathematics and Systems Science, Chinese Academy of Sciences from 2010 to 2013. Now, he is a project stuff at the relativity group of the Morningside Center of Mathematics and the Institute of Applied Mathematics, Chinese Academy of Sciences. His research interests now include relativistic experiments in space, satellite gravity, gravitational wave physics and the related noise simulations and data analysis techniques.